Journal of Neuroinflammation

RESEARCH

Open Access

Integration and functionality of human iPSC-derived microglia in a chimeric mouse retinal model

Chun Tang[1,2†], Qi-Qi Zhou[1,2†], Xiu-Feng Huang[3†], Ya-Yi Ju[1,2], Bi-Lin Rao[1,2], Zhi-Cong Liu[1,2], Yi-An Jia[1,2], Zhan-Pei Bai[3], Qing-Yang Lin[1,2], Lin Liu[1,2], Jia Qu[1,4*], Jun Zhang[1,2,5*] and Mei-Ling Gao[1,2,6*]

Abstract

Introduction Microglia, the resident immune cells of the central nervous system, play a pivotal role in maintaining homeostasis, responding to injury, and modulating neuroinflammation. However, the limitations of rodent models in accurately representing human microglia have posed significant challenges in the study of retinal diseases.

Methods PLX5622 was used to eliminate endogenous microglia in mice through oral and intraperitoneal administration, followed by transplantation of human induced pluripotent stem cell-derived microglia (hiPSC-microglia, iMG) into retinal explants to create a novel ex vivo chimeric model containing xenotransplanted microglia (xMG). The number and proportion of xMG in the retina were quantified using retinal flat-mounting and immunostaining. To evaluate the proliferative capacity and synaptic pruning ability of xMG, the expression of Ki-67 and the phagocytosis of synaptic proteins SV2 and PSD95 was assessed. The chimeric model was stimulated with LPS, and single-cell RNA sequencing (scRNA-seq) was used to analyze transcriptomic changes in iMG and xMG. Mouse IL-34 antibody neutralization experiments were performed, and the behavior of xMG in retinal degenerative Pde6b$^{-/-}$ mice was examined.

Results We demonstrated that xenotransplanted microglia (xMG) successfully migrated to and localized within the mouse retina, adopting homeostatic morphologies. Our approach achieved over 86% integration of human microglia, which maintained key functions including proliferation, immune responsiveness, and synaptic pruning over a 14-day culture period. scRNA-seq of xMG revealed a shift in microglial signatures compared to monoculture iMG, indicating a transition to a more in vivo-like phenotype. In retinal degenerative Pde6b$^{-/-}$ mice, xMG exhibited activation and migrated toward degenerated photoreceptors.

†Chun Tang, Qi-Qi Zhou and Xiu-Feng Huang contributed equally to this work.

*Correspondence:
Jia Qu
jia.qu@eye.ac.cn
Jun Zhang
zj9999@eye.ac.cn
Mei-Ling Gao
gaoml@wmu.edu.cn

Full list of author information is available at the end of the article

Conclusion This model provides a powerful platform for studying human microglia in the retinal context, offering significant insights for advancing research into retinal degenerative diseases and developing potential therapeutic strategies. Future applications of this model include using patient-derived iPSCs to investigate disease-specific microglial behaviors, thereby enhancing our understanding of microglia-related pathogenesis.

Graphical abstract

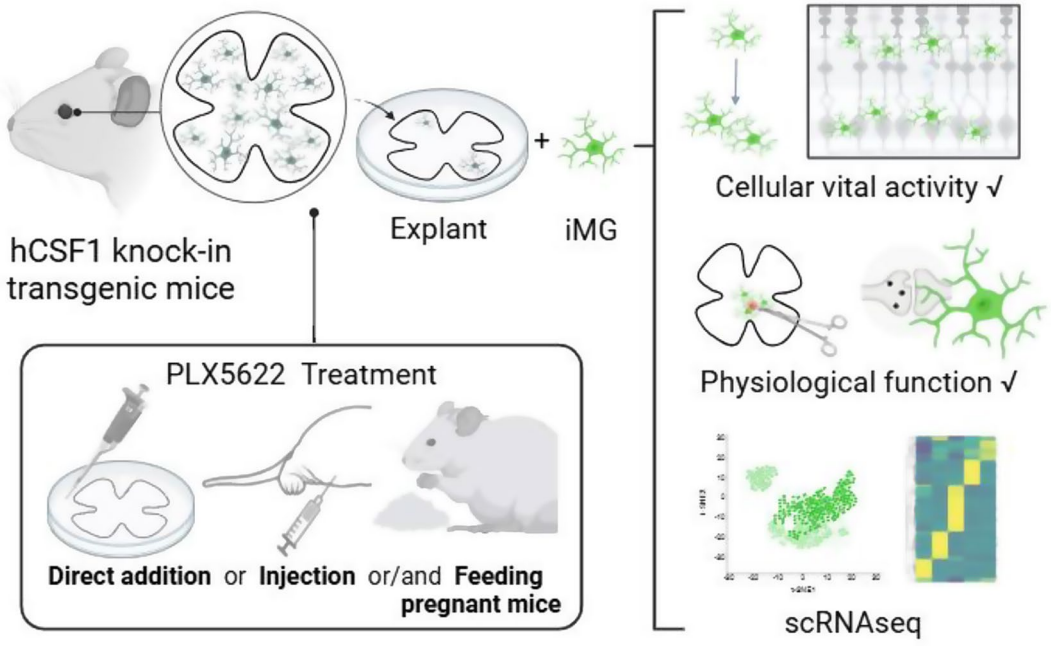

Keywords Microglia, Xenotransplantation, HiPSCs, Retinal explant, Chimeric

Introduction

Microglia, the resident immune cells of the central nervous system (CNS) are crucial for maintaining homeostasis, defending against pathogens, and providing neuroprotection in various pathological conditions [1]. They actively participate in inflammation, tissue repair, and synaptic remodeling, which are crucial for maintaining the balance of the CNS microenvironment [2, 3]. Furthermore, microglia have been implicated in the pathogenesis of various retinal disorders, including glaucoma, age-related macular degeneration (AMD), optic neuropathy, retinitis pigmentosa, uveitis, and diabetic retinopathy [4, 5]. Genome-wide association analysis has identified several genes associated with the pathogenesis of AMD, including CFH, C2, and C3 [6–8], which are notably expressed in microglia [9].

Recent studies highlight significant differences in gene expression between mouse and human microglia, raising concerns about the accuracy of rodent models in representing human microglia [10–12]. The expression level of certain disease-related genes is significantly different in human microglia and murine microglia, emphasizing the limitations of relying solely on rodent models [13]. Moreover, the difficulty in obtaining human primary microglia and the challenges associated with ex vivo cultures, which often exhibit a marked downregulation of homeostatic genes, underscore the need for more relevant human microglia models in scientific and clinical research [12, 14]. In response to this demand, protocols for differentiating microglia-like cells (iMG) from induced pluripotent stem cells (iPSCs) have been established, providing a valuable tool for studying microglia biology [15–18]. Although iMG closely resemble primary microglia in phenotype and function, discrepancies persist in the expression of homeostatic genes [19]. To mitigate this disparity, researchers have endeavored to transplant iMG into mouse brains and retina, resulting in chimeric microglia (xMG) [19–22]. The expression of homeostatic genes in xMG becomes progressively more akin to primary microglia over time [23], providing a robust platform for studying the role of microglia in disease and screening new drugs targeted microglia.

Despite these advancements, in vivo transplantation poses significant challenges, including the complexities of raising and breeding transgenic mice, the technical difficulties of transplantation surgery, particularly subretinal

injection, and the necessity of using immunodeficient animals to avoid immune rejection [19–23]. The knockout of immune-related genes in these animals, and the resulting changes in immune function, may render them unsuitable for certain types of research or drug screening [24]. Given these limitations, developing an ex vivo model that bypasses the need for immunodeficient animals is a promising alternative [25]. Success in isolating and culturing both animal retinal explants and donated human retinal tissue ex vivo offers a compelling platform for studying retinal damage and degenerative diseases [26, 27].

This study introduces a novel approach in which human iPSC-derived microglia are transplanted into mouse retinal explants to create a human microglia-mouse retina chimeric model. This model successfully integrates human microglia into the mouse retina, where they adopt mature morphologies and migration patterns similar to native microglia. To deplete endogenous mouse microglia, two different PLX5622 treatment methods were employed in this study, resulting in xMG replacement efficiencies of approximately 50% and over 80%, respectively. The transplanted human microglia respond to immune stimuli, such as lipopolysaccharide (LPS) and injury signals, and engage in synaptic pruning by phagocytosing mouse synapses. Additionally, the localization of xMG within the retina appears to be dependent on IL-34 signaling. Single-cell RNA sequencing (scRNAseq) reveals a shift in the microglial signature profile of xMG compared to monoculture iMG. In the Pde6b$^{-/-}$ retina, xMG showed ameba-like morphology in the outer nuclear layer (ONL), where degenerative photoreceptors are located, indicating their activation in the retinal degenerative condition. These findings demonstrate the potential of this chimeric model as a valuable tool for exploring the role of human retinal microglia in both normal physiology and disease conditions.

Materials and methods

Animals

All experimental animals were raised in the Specific Pathogen-Free (SPF) animal facility of the Experimental Animal Center of Wenzhou Medical University. The animal experiment procedures were conducted in accordance with the guidelines approved by the Animal Ethics Committee of Wenzhou Medical University (approval number wydw2023-0321). Transgenic mice (Rag2$^{-/-}$; Il2rg$^{-/-}$; hCSF1$^{+/+}$) were purchased from the Jackson Laboratory (Stock No: 017708), while BALB/c mice were purchased from GemPharmatech Co., Ltd (Jiangsu, China). The transgenic mice were bred with BALB/c mice to produce hCSF1$^{+/+}$ mice. hCSF1$^{+/+}$ mice were used for subsequent retinal explant.

Pde6b$^{-/-}$ mice, exhibiting a severe early-onset retinal degeneration phenotype, were obtained from Cyagen (Cat.# C001384, China). All animals were maintained under controlled conditions with 12 h light-dark cycle at 22 °C.

Human iPSC culture

The hiPSCs and hiPSC-EGFP, labeled by nuclear-expressed EGFP, were obtained from Nuwacell (Cat.# RC01001-A, RC01009, China). The cells were cultured on Matrigel-coated (Cat.# 354277, Corning) six-well plates with ncTarget medium (Cat.# RP01020, Nuwacell, China). Upon reaching approximately 85% confluence, the cells were passaged using 0.5 mM EDTA solution (Cat.# RP01007, Nuwacell). Following passage, the cells were maintained in a fresh medium supplemented with 1.5 μg/ml blebbistatin (Cat.# RP01008, Nuwacell), a ROCK inhibitor. Using these hiPSC, hiPSCs-RFP were generated with RFP lentivirus obtained from WZ Bioscience Inc. (Cat.# LV100015-OE, China). Mycoplasma contamination was tested bi-monthly, and only mycoplasma-negative cells were used in subsequent experiments.

Generation of hiPSC-derived microglia

To differentiate microglia-like cells from hiPSCs, both hiPSC-EGFP and hiPSCs-RFP were used following the protocol described previously [28, 29]. Briefly, when iPSCs reached approximately 85% confluence in six-well plates, they were dissociated with 0.5mM EDTA solution (Nuwacell) and then cultured in suspension in advanced DMEM/F12 medium (Cat.# 12634010, Gibco, USA) supplemented with 10% KnockOut SR (Cat.#10828028, Gibco, USA), 2mM GlutaMAX (Cat.# 35050-061, Gibco), 100U/ml Pen/100μg/ml Strep (Cat.# 10378016, Gibco, USA), 0.1mM β-mercaptoethanol (Cat.# M6250, Sigma-Aldrich, USA) and 1.5 μg/ml blebbistatin (Nuwacell). On differentiation day 4, the embryoid bodies (EBs) were transferred to a 100 mm dish pre-coated with 0.1% gelatin (Cat.# es-006-B, Merck Sigma) using Lonza X-vivo 15 plus medium (Cat.# 04-418Q, Lonza, USA) supplemented with 2mM GlutaMAX, 100U/ml Pen/100μg/ml Strep, 0.1mM β-mercaptoethanol, 25ng/ml hrIL-3 (Cat.# 203-IL-050, R&D Systems, USA) and 50ng/ml hrM-CSF (Cat.# 216-MC-500, R&D Systems). The medium was then changed every 7 days. After approximately one month, hematopoietic progenitor cells were generated and suspended in the medium. The suspended cells were carefully collected and subjected to iMG differentiation in the medium consisting of DMEM/F12 (Cat.# 10565018, Gibco, USA) and neurobasal medium (Cat.# 21103049, Gibco, USA) containing 1% B27 supplement (Cat.# RC01026, Nuwacell), 0.5% N2 supplement (Cat.# 17502-048, Gibco, USA), 2mM GlutaMax and 0.1mM

β-mercaptoethanol, supplemented with 100ng/ml hrM-CSF (R&D Systems, USA) and100ng/ml hrIL-34 (Cat.# 200 – 34, PeproTech, USA).

Western blotting

Synaptosome was extracted from mouse brain using Syn-PER Synaptic Protein Extraction Reagent (Cat.# 87793, Thermo Fisher Scientific). Protein concentrations were determined using BCA kit (Cat.# P0012, Beyotime). Samples containing 51 μg of protein were heated at 95 ℃ for 10 min and separated on a 10% SDS-polyacrylamide gel. Protein bands were transferred to a polyvinylidine difluoride (PVDF) membrane. The membrane was blocked with blocking solution and then incubated with primary antibodies against SV2 (Cat.# 62602, Monoclonal RRID: B_2315387, DSHB), Synaptophysin (Cat.# MAB5258-I, clone SY38, Merck Millipore), and β-actin (Cat.# AF0003, Beyotime, China) overnight at 4℃. After three washes with TBST, the membrane was incubated with horseradish peroxidase (HRP)-conjugated secondary antibodies for 2 h at 37 °C. Signals were detected using enhanced chemiluminescence (ECL) and the iBright CL1500 imaging system (Thermo Fisher Scientific).

Assessment of iMG phagocytosis

iMG, induced for 7 days, were then cultured on glass slides for an additional 7 days. Subsequently, to qualitative assessment of iMG phagocytosis, beads or synaptosomes were added directly to iMG culture medium. The cells were further incubation at 37 °C for 6 h. The cells were fixed and subjected to immunofluorescence to observe the phagocytosis.

Immunofluorescence

Explant retinas were embedded in embedding reagent (Sakura Finetek) and subjected to cryo-sectioning. The cells, sections or retina were fixed with 4% paraformaldehyde (PFA) and blocked with 5% normal donkey serum containing 0.3% Triton X-100 for 2 h at room temperature. Next, the primary antibodies, including Iba1 (1:400, Cat.# 019-19741, Wako), SV2 (1:200, DSHB), PSD95 (1:100, Cat.# ab12093, Abacm), PKCα (1:300, Cat.# 610107, BD Transduction Laboratories), Ki-67 (1:200, Cat.# 556003, BD Biosciences), GFAP (1:400, Cat.# HPA056030, Sigma), hTMEM119 (1:100, Cat.# PA5-62505, Thermo Fisher Scientific), was diluted in blocking solution and incubated with the cells, sections or retina overnight at 4℃. Following primary antibody incubation, the cells, sections or retina were washed and then incubated with appropriate secondary antibodies (1:500) and DAPI (1:5000) for at least 2 h at room temperature. Imaging was performed using a Zeiss LSM900 confocal microscope.

Quantitative PCR (qPCR)

According to the manufacturer's protocol, total RNA was isolated from iMG and retinal explants using Trizol reagent (Cat.# 15596018CN, Thermo Fisher Scientific). Subsequently, 1 μg of RNA was reverse transcribed to cDNA using HiScript III RT SuperMix for qPCR (+gDNA wiper) kit (Cat.# R323-01, Vazyme). The fluorescence from SYBR Green I (Cat.# Q712-03, Vazyme) was detected using a real-time PCR system (QuantStudio 3, Thermo Fisher Scientific Applied Biosystems). The expression levels of TMEM119, CX3CR1, P2RY12, OCT-4, hIL-1β, hTNF-α, hIL-6, hARG1, hMCP-1 mRNAs were normalized to that of RPL13A and mIl-1β, mTnf-α, mIl-6, mArg1, mMcp-1 were normalized to that of mGapdh. Primer sequences are listed in Table S1.

Transmission electron microscope (TEM)

The samples (iMG) were fixed with 2% glutaraldehyde (Cat.# 16020, Electron Microscopy Sciences) and 2% PFA (Cat.# 157-8, Electron Microscopy Sciences) in 0.1 M phosphate buffer for 6 h with shaking at room temperature, followed by overnight at 4℃ [30]. After six washes in PBS, the samples were treated with 1% osmium tetroxide (Cat.# 20816-12-0, Electron Microscopy Sciences) for 30 min at 4℃. Subsequently, the samples were washed and then incubated in uranyl acetate (Cat.# 541-09-3, Electron Microscopy Sciences) for 1 h at room temperature, avoiding light, for staining. For dehydration, the cells were dehydrated in a gradient of 50%, 70%, 80%, 90% and 100% (twice) ethanol, followed by the addition of Epon-815 resin (Electron Microscopy Sciences) and ethanol in a 1:1 ratio at 37℃. Following this, the ratio of Epon resin to ethanol was adjusted to 4:1, and the cells were incubated in a 37℃ oven overnight. The next day, the samples were embedded pure Epon resin and placed in a 54℃ oven for 1 h. Subsequently, the cells were polymerized with fresh embedding medium for 48 h. For retinal explants, acetone was used instead of ethanol in the dehydration process.

Immuno-EM

The retinal explants were fixed with 4% PFA (Electron Microscopy sciences) and 0.2% glutaraldehyde (Electron Microscopy Sciences) in 0.1 M phosphate buffer for 2 h with shaking at room temperature, then transferred in 4% PFA in 0.1 M phosphate buffer for 3 h with shaking at room temperature. After ten washes in PBS, the samples were incubated with 5% normal goat serum (NGS) for 30 min at room temperature. Next, the samples were incubated in anti-GFP primary antibody (1:400, Cat.# MAB3580, Millipore) in PB containing 5% NGS for 2 h at room temperature, followed by 3 days at 4℃. After ten washes in PBS, the samples were incubated with secondary antibody 1:100 (goat anti-mouse IgG) for 2 h,

on shaker; then 4 days at 4℃. After being washed, the samples were treated in ABC solution (0.01%A solution, 0.01%B solution in PBS) for 2 days at 4℃. Then the samples were stained by DAB solution for with 0.01% H_2O_2. After ten washes in PBS, the samples were processed with routine TEM processes as mentioned above.

Depletion of microglia in mouse retina

To establish microglia-free niches, we employed three methods to deliver PLX5622 (PLX, Cat.# S8874, Selleck), a CSF1R inhibitor. PLX powder was dissolved in DMSO to prepare a 60 mg/mL stock solution. Firstly, retinal explants from postnatal day 7 (P7) mice were cultured in a medium containing PLX (3 μM) for either 24–72 h immediately after dissection. Secondary, neonatal mice (P1) were intraperitoneally injected at a dosage of 200 mg per kg of mouse body weight for 4 consecutive days. Thirdly, pregnant mice were orally administered PLX (4.8 mg/day in feed) for 10 days. The offsprings were either intraperitoneally injected with 200 mg/kg PLX for an additional 4 more days or used for retinal explant culture directly for longer-term culture.

Retinal explants culture and iMG transplantation

Neonatal mice were anaesthetized on ice and then euthanized. Retinas were carefully dissected and cut into four-leaf clover shapes. The retinas were placed on a PV membrane (Cat.# GTTP01300, Merck) with the photoreceptor cell layer facing the membrane in 2 ml/well DMEM medium containing DMEM/F12(3:1) (Gibco), Neurobasal medium (Gibco), 2mMGlutaMAX (Gibco), 0.5 mg/ml Pen/Strep (Gibco), NEAA (Cat.# M7145, Sigma-Aldrich), and B27 supplement (Nuwacell) in 12-well plate. The entire membrane with the retina was transferred to a 12-well culture plate containing medium. The plate was then placed in a sterile incubator at 37 ℃ with 5% CO_2. It's important to ensure that the retina remains at the liquid-air interface on the membrane. Approximately 1 h after dissection, a total of 16,000 iMG in 10 μl of medium were added to the ganglion cell layer surface of the retina. Half of the fresh medium was replaced daily to maintain the cultural conditions. For $hCSF1^{+/+}$ mice, forced expression of hCSF was sufficient to support the survival of xMG, but additional 100 ng/ml hrIL-34 (Cat.# 200 – 34, PeproTech) was required in the retinas of $Pde6b^{-/-}$ mice.

Antibody neutralization

Pregnant mice were orally administered PLX (4.8 mg/day in the feed) for 5 days, and the newborn mice received intraperitoneal injections of 200 mg/kg PLX for an additional 4 days. Retinas were dissected in sterile DPBS and placed on a PV membrane as previously described, then cultured in a medium containing 0.5 μg/ml mouse IL-34 antibody (Cat.# AF5195-SP, R&D Systems). After 24 h, 32,000 iMG in 10 μl of medium were added to the ganglion cell layer of the retina, and the culture was continued for an additional 3 days. Fresh medium containing mouse IL-34 antibody was replaced daily.

Isolation of xMG

Retinal explants after transplanted for 7 days were washed with DPBS and immersed in a dissociation buffer containing 20 U/mL papain (Cat.# LK003178, Worthington, Germany) and 0.5 mg/mL DNase I (Cat.# 11284932001, Roche) for 12–15 min at 37 °C. The homogenate was then pelleted and filtered through a 40 μm filter. After centrifugation at 300×g for 5 min, the cell pellets were resuspended in DPBS. The centrifugation was repeated, and the cells were resuspended in DPBS containing DNase I, and a transcription inhibitor cocktail, which included 5 μg/mL Actinomycin D (Cat.# HY-17559, MedChemExpress, USA), 10 μM Triptolide (Cat.# HY-32735, MedChemExpress, USA), and 27.1 μg/mL Anisomycin (Cat.# HY18982, MedChemExpress, USA). RFP-positive xMG were sorted at 7 days after transplantation using flow cytometry (CytoFLEX LX, Beckman Coulter, USA).

Single-cell RNA sequencing (scRNA-seq) and data analysis

Sorted xMG or dissociated iMG were subjected to scRNA-seq using a 10× Genomics instrument with the 10X Genomics Chromium Single-Cell 3′ kit (V3), following the manufacturer's instructions. Full-length cDNA and library construction were performed according to the established protocol by LC-Bio Technology Co., Ltd, (Hangzhou, China). The libraries were sequenced using the Illumina NovaSeq 6000 sequencing system at a minimum depth of 20,000 reads per cell.

Raw sequencing data were preprocessed using the CellRanger software (v7.2.0, 10X Genomics) to generate gene expression matrices. Seurat (v4.4.1) was applied for downstream data integration and analysis. To filter out potential empty droplets, low-quality cells, and multiplets, quality control measures were implemented to exclude cells with more than 5000 detected genes, over 20,000 mRNA molecules, or mitochondrial ratio greater than 10%. Harmony (v1.2.0) was employed to remove contaminated mouse cells and for batch effect correction. The LogNormalize method of the "Normalization" function in Seurat software was applied for visualization. Differential gene expression analysis was subsequently carried out using the FindAllMarkers() function in Seurat, applying a default two-sided nonparametric Wilcoxon rank sum test to compare one cluster with the others. Genes with a log-scaled fold change ≥ 0.58 (log2 (1.5)) and an adjusted P-value < 0.05 were deemed significant.To investigate the potential functions of the selected gene list and cluster markers, we employed the

clusterProfiler R package (v4.8.3) in combination with the msigdbr R package to retrieve pathway gene sets from the Molecular Signature Database (https://www.gsea-msigdb.org/gsea/msigdb/). These gene sets, sourced from the Gene Ontology and Kyoto Encyclopedia of Genes and Genomes (KEGG) databases, were used to enrich the selected gene list. Significance was assessed using an adjusted *P*-value threshold of <0.05. CellChat (v1.6.1) was employed to infer cell-cell communication and identify specific ligand-receptor pairs. The communication probability between two clusters was calculated based on the average expression levels of ligands in one cluster and receptors in the other. Significance of communication was evaluated using permutation tests.

Graphics and statistical analysis

The graphic abstract figure and the schematic images in figures and supplementary figures are created in BioRender. Liu, Z. (2024) BioRender.com/c78b112. Confocal images were processed for 3D reconstruction using Imaris software. Statistical analyses and data visualization were conducted using GraphPad Prism9. All variables are presented as mean ± standard deviation (SD). Significant differences were determined using unpaired two-tailed Student's t-test or one-way ANOVA. $P<0.05$ was considered statistically significant.

Results

Generation and characterization of iMG

We generated iMG-EGFP and -RFP, with EGFP specifically expressed in the nucleus and RFP distributed throughout the cytoplasm, following an established protocol (Fig. S1A, B) [28, 29]. The resulting iMG exhibited complex branching structures and expressed key microglial markers, including P2RY12 and IBA1 (Fig. S1C). Importantly, the iMG showed significant enrichment of microglial-specific genes such as CX3CR1, TMEM119, and P2RY12, while the pluripotency marker OCT-4 was no longer detected (Fig. S1D). To assess the phagocytic capacity of iMG, we conducted engulfment assays using fluorescent nano-beads. Both immunofluorescence and transmission electron microscopy (TEM) confirmed that iMG effectively took up a substantial number of beads (Fig. S1E, F). Furthermore, when exposed to purified synaptosomes, iMG demonstrated significant uptake of synaptosomes (Fig. S1G, H). Overall, we successfully obtained a sufficient quantity of high-quality iMG for further experimentation.

xMG resident in the mouse retina explant

Colony-stimulating factor 1 receptor (CSF1R) signaling is essential for microglia survival [31]. Due to species-specific differences, mouse CSF1 cannot support human microglia survival [32]. Therefore, we employed human CSF1 knock-in transgenic ($hCSF1^{+/+}$) mice to generate explant retinas to support the survival of xenotransplanted iMG (xMG). To create a microglia-free niche, we depleted endogenous mouse microglia using PLX5622 (PLX), a CSF1R inhibitor (Fig. S2A). Retinas were dissected from neonatal mice (P7) and directly cultured in a medium containing 3μM PLX. After 24 and 72 h of culture, we observed a significant increase in microglial depletion in the 72 h group compared to the 24 h group (Fig. S2B). Following PLX treatment, 10 μl of 16,000 iMG were added to the inner surface of mouse organotypic retinal explants and cultured in fresh medium without PLX. The survival of transplanted xMG was minimal in the 24 h PLX-treated group but significantly increased in the 72 h group after 1 day post-transplantation (d.p.t) (Fig. S2C). However, xMG primarily survived in the periphery of the retina, where endogenous microglia had been eliminated at 1 d.p.t. Over 3 d.p.t, iMG gradually migrated from the periphery toward the center (Fig. S2C). Despite this migration, regional variability in distribution persisted due to the unequal depletion of resident microglia (Fig. S2D), which might be influenced by the penitrition of PLX. These findings demonstrate that xMG can survive and migrate within mouse retinal explants when hCSF1 knock-in retinas are used; however, immunodeficient mice are not required for xMG survival. Notably, the distribution of xMG depends on the presence of a microglia-free niche.

xMG resemble native microglia in the mouse retina explant

To address the uneven microglial depletion, we administered intraperitoneal PLX injections to newborn mice, achieving a more uniform elimination of retinal microglia before culturing the retinal explants and transplanting iMG (Fig. 1A). This approach resulted in approximately 49.22% depletion of retinal microglia (Fig. 1B-D). Consequently, xMG were evenly distributed within the explant retina. By 3 d.p.t., most xMG exhibited a rounded morphology, transitioning to a branched morphology by 7 d.p.t. (Fig. 1E, F). Although the overall cell count did not significantly different between 3 and 7 d.p.t., the number of surviving xMG varied among individual retinas, stabilizing nearly 2,000 cells at 7 d.p.t. (Fig. 1G). xMG coexisted with mouse microglia, with their combined total closely resembling the retinal microglial count in untreated mice (Fig. 1H).

Our previous studies indicated that approximately 12% of cultured iMG possess the ability to replicate [28]. To investigate whether xMG retain this replicative capacity in the retina, we used the Ki-67 antibody to label proliferating cells. We observed both EGFP and Ki-67 positive human microglia at 3 and 7 d.p.t. (Fig. 1I), with similar proportions of Ki-67 positive xMG at both time points (Fig. 1J). This suggests that xMG can sustain

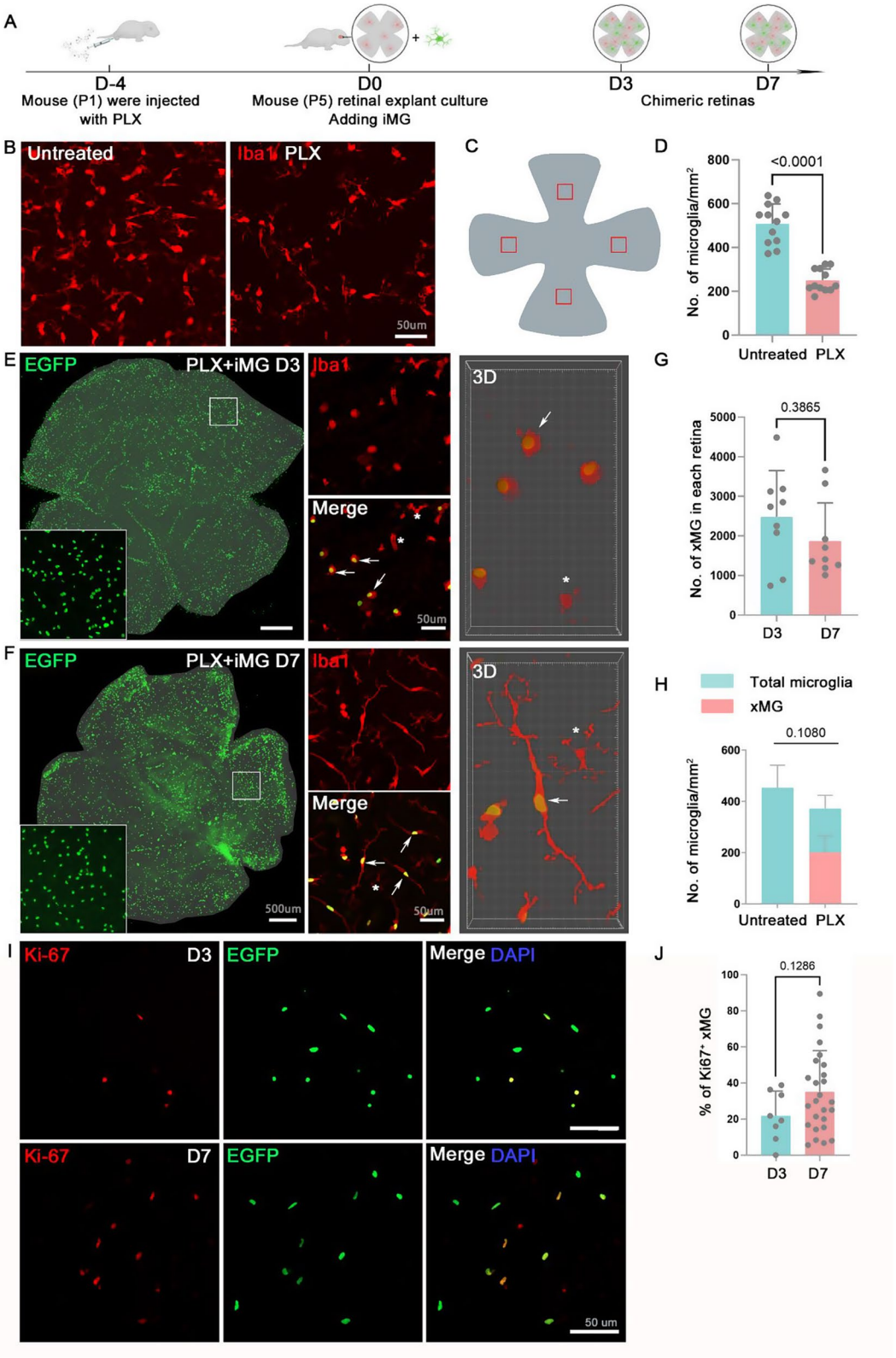

Fig. 1 (See legend on next page.)

(See figure on previous page.)

Fig. 1 Development and integration of human iPSC-derived microglia in ex vivo mouse retinal explants. (**A**) Schematic diagram illustrating experimental methods and procedures. Neonatal mice are administrated with PLX5622 for 4 days, followed by retina explant culture. iMG (16000 iMG/retina) are added from the retinal ganglion cell layer immediately following dissection. (**B**) Immunofluorescence images of anti-Iba1 (red) showing the distribution of endogenous mouse microglia (mMG) in retina following PLX5622 administration. Scale bars, 50 μm. (**C**) Schematic diagram of areas photographed for statistical analysis of microglia density. (**D**) Quantifications of mouse microglia density in untreated and PLX5622 treated groups. $n = 3$ retinas. (**E**, **F**) The distribution of xMG (GFP^+ $IBA1^+$) and mMG (GFP^- $IBA1^+$) in mouse retina explants at 3 or 7 days post-transplantation. Arrows indicate xMG. Stars indicate mMG. Scale bars, 500 μm (orignal images) or 50 μm (amplified images). (**G**) Quantifications of xMG in mouse retina after transplantation for 3 and 7 days. $n = 3$ retinas. (**H**) The density of xMG and total microglia (xMG and mMG) in mouse retina explants after coculturing 7 days. (**I**) Representative immunofluorescence images of anti-Ki-67 (red) and EGFP labeled xMG (green) in retinas post-transplanted for 3 or 7 days. Scale bars, 50 μm. (**J**) Quantifications of the percentage of $Ki\text{-}67^+$ xMG in total xMG cells in mouse retinal explants post-coculture for 3 or 7 days. $n = 3$–7 retinas

their replicative ability for a period within mouse retina explants.

xMG perform synaptic pruning and respond to stimulation

Given the role of microglia in promoting neuronal development through synaptic pruning [33], we investigated whether xMG affects synapse development in the chimeric model. We first assessed the expression of the synaptic vesicle protein SV2 and the postsynaptic protein PSD95 in retinal explants at various time points. The results showed that, prominent SV2 and PSD95 bands formed in the outer plexiform layer (Fig. 2A), resembling the in vivo pattern [34]. This finding suggests that transplantation of xMG, following the elimination of endogenous microglia in mice, does not significantly impact synaptic development. Additionally, phagocytic SV2 and PSD95 signals were observed in the xMG, indicating that xMG may contribute to synaptic pruning in retinal explants (Fig. 2B, C).

To assess the ultrastructure of xMG, we conducted immuno-EM targeting EGFP to investigate xMG development within the chimeric model. xMG was obviously identified by its nucleus stained completely by DAB reaction product with high electron density (Fig. 2D). In contrast, mouse microglia, without DAB labeling, showed a distinct separation between euchromatin and heterochromatin (Fig. 2D). Based on this, numerous xMGs with rich organelles such as mitochondria were visible throughout the chimeric model.

To evaluate xMG' response to immune stimulation, we treated the chimeric retinas with LPS and analyzed the transcriptomic changes of inflammatory genes specific to humans and mice. Human genes IL-1β, IL-6, and TNF-α were upregulated in the LPS-treated group, with a similar trend observed in their mouse counterparts, except for Arg-1 (Fig. 2E). These results suggested that LPS can elicit a proinflammatory response in both human and mouse microglia. Differences in MCP-1/mMcp-1 expression between species were also noted, with significant mMcp-1 increase and slight MCP-1 decrease (Fig. 2F). Mcp-1 are mainly secreted by astrocytes [35–37], and the increased mMcp-1 may result from astrocyte activation. Additionally, the morphology of xMG underwent a dramatic transformation following LPS treatment (Fig. 2G, H). Upon stimulation, xMG branches retracted, adopting an ameboid-like shape, indicative of an activated microglial state in response to inflammatory signaling. These findings indicate that xMG are responsive to LPS stimulation in mouse retina explants.

Neural retinal microenvironment induces transcriptional changes in xMG

To explore how the retinal microenvironment influences transplanted xMG, we performed scRNA-seq by dissociating iMG at differentiation day 14 and sorting xMG at 7 d.p.t. A total of 13,504 single cells were obtained after quality control, including 9,832 iMG and 3,222 xMG (Fig. 3A and S3A). We excluded 5% of the cells due to artifactual changes during single-cell preparation [38]. Both samples displayed enriched microglial signature genes with minimal pluripotency markers (Fig. S3C, D), confirming their microglial identity. The retinal microenvironment significantly altered the xMG transcriptional signature (Fig. 3B, C). In xMG, highly expressed genes were linked to neural development, such as regulation of nervous system development and synaptic plasticity, while immune response-related genes were enriched in iMG (Fig. S3E, F).

Uniform manifold approximation and projection (UMAP) analysis identified five clusters (Fig. 3A and S3G), reflecting transcriptional diversity similar to a previous report with iMG exposure to different neuronal components [39]. Four clusters corresponded to previously defined microglial states: DAM (LPL and CD9), pro-inflammatory (IL1B, CCL4, and TNF), homeostatic (P2RY12 and FSCN1), and proliferative (TOP2A and STMN1). A small proportion of stress-responsive states, specific to the retina, were identified, expressing genes like ITGAX, VMP1, and NAMPT (Fig. 3D, E).

Ligand and receptor interaction are critical for microglia to sense environmental changes [40, 41]. Thus, we next analyzed the cell-cell communication with ligand and receptor interaction between different cell states in both iMG and xMG (Fig. S4A). The microglial activation-related signaling, such as CCL8/CCL3/CCL13-CCR1 and SPP1-CD44 signaling was significantly higher in iMG than that in xMG (Fig. S4A). Especially, the homeostatic xMG expressed significantly lower ligands of CCL

signaling in xMG than that in iMG (Fig. 3F, S4B), and similar of SPP1 signalling in xMG and iMG (Fig. S4C). Among these five clusters, the homeostatic state is predominant in both iMG and xMG (Fig. 3B). Thus, we compare the transcriptional signature of homeostatic iMG and xMG to elucidate the context-dependent changes (Fig. S4A). The expression of antigen processing related GO terms were significantly enriched in homeostatic xMG, and immune response-related GO terms were significantly enriched in homeostatic iMG (Fig. 3G, H, S5). These findings underscore the retinal microenvironment's significant impact on xMG transcription, highlighting their specialized role in the retina.

xMG effectively replace mouse microglia in mouse retina explants

To enhance microglial elimination, we supplemented the diet of pregnant mice with PLX and administered intraperitoneal injections after birth (Fig. 4A). In subsequent ex vivo culture, xMG demonstrated improved survival within retina explants, achieving approximately 86.72% replacement in the ganglion cell layer (GCL) and inner plexiform layer (IPL) and 97.19% replacement in the OPL (Fig. 4B, C). xMG predominantly localized to the OPL, IPL, and GCL, closely mirroring their in vivo distribution. xMG morphology varied by retinal location, with more branching in the GCL/IPL and spindle-shaped or rod-shaped cells in the OPL. xMG in the outer nuclear layer (ONL) appeared rounded with fewer protrusions (Fig. 4D, E). The number of xMG in the GCL/IPL was comparable to that in the OPL (Fig. 4F). These results demonstrate the effectiveness of xMG replacement and successful integration into retinal tissue.

The retina contains two distinct microglia pools that differ in niche and dependency on interleukin-34 (IL-34) signaling, with the IPL serving as an IL-34-dependent niche [42]. To investigate whether xMG are influenced by IL-34 signaling, we blocked murine IL-34 signaling using an anti-mouse IL-34 antibody (Fig. 4G). In the anti-IL-34 group, the number of xMG in the IPL significantly reduced by 54.5%, while no significant reduction was observed in the GCL (Fig. 4H). The number of xMG in the OPL was also affected by anti-IL-34 treatment (Fig. 4H), likely because iMG were initially added to the GCL and had to migrate through the IPL to reach the OPL. These results suggest that xMG migration and localization are dependent on IL-34 signaling, demonstrating that xMG can effectively replace mouse microglia and mimic in vivo microglial distribution.

Longer-term culture of mouse retinal explants with functional xMG

Despite improved xMG replacement efficiency, short culture times limited the detection of microglia homeostasis-related proteins. Previous studies reported that retinal explants could be maintained for 14 days [43, 44]. Therefore, we aimed to establish a longer-term culture of retinal chimeric models ex vivo (Fig. 5A). We administered PLX orally to pregnant mice to eliminate microglia in the retina, resulting in retinal explants obtained from the newborn (P1) mice with 85% microglial depletion (Fig. 5B). Following 14 days of culture, mouse retinal explants developed into typical retinal structures, with xMG localizing to the IPL, OPL, and GCL where endogenous microglia reside (Fig. 5C). In 14-day-old chimeric mouse retinal explants, the expression of TMEM119 was observed in xMG (Fig. 5D). This is consistent with mouse microglia, which exhibit similar expression levels of TMEM119 to adult levels at P14 [45]. Furthermore, xMG retained the ability to proliferate, with the proportion of Ki-67-positive cells similar to that observed after 7 days of culture (Fig. 5E). However, the xMG replacement rate reached 83% on the seventh day of culture, but dropped to 70% on the 14th day (Fig. 5F). Additionally, after 14 days of culture, the number of xMG cells in the OPL significantly increased, surpassing the number of cells in the GCL/IPL (Fig. 5G). These findings emphasize the importance of prolonged culture durations for a comprehensive evaluation of xMG behavior and functionality within retinal chimeric models.

To assess mature xMG' response to injury, we induced tissue damage in the retina using a needle and observed xMG distribution after 2 h. In non-injury controls, xMG were scattered throughout the retina, while they clustered near injury sites (Fig. 6A). xMG at injury sites exhibited a rounded morphology with CD68-positive puncta, indicating phagocytic activity (Fig. 6B). We also examined the interaction between xMG and synaptic proteins, focusing on the postsynaptic protein PSD95. Mature xMG with ramified morphology were observed in contact with synaptic proteins, with engulfed synaptic proteins detected inside the xMG (Fig. 6C). These findings suggest that mature xMG retain the ability to respond to injury and effectively prune synapses.

Responsive xMG in Pde6b−/− retinal explants

Previous studies have shown microglial activation in retinal degenerative conditions [46]. To further investigate this, we used the Pde6b$^{-/-}$ mouse model, which mimics early-onset retinitis pigmentosa and exhibits significant ONL loss by P22, similar to the *rd1* phenotype (Fig. S6). We cultured neonatal (P5) Pde6b$^{-/-}$ retinas and added iMG as wild-type (WT) controls. Seven d.p.t, xMG predominantly localized to the ONL/OPL and RGCL/IPL regions of the Pde6b$^{-/-}$ retina (Fig. 7A). In the ONL/OPL of the Pde6b$^{-/-}$ retina, xMG exhibited an amoeba-like morphology, indicative of activation, whereas in the WT retina, xMG displayed a ramified morphology

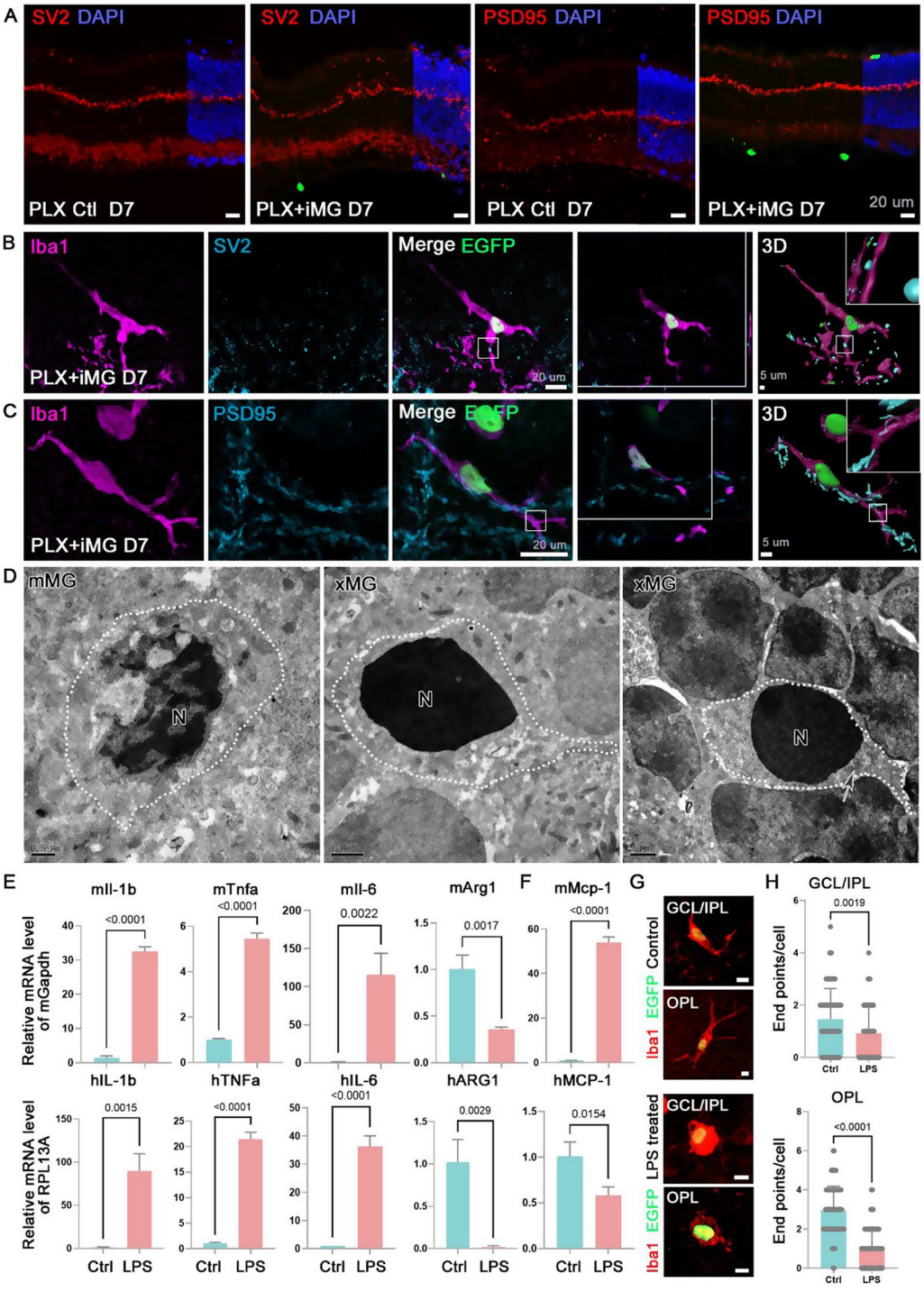

Fig. 2 xMG phagocyte synaptic proteins and response to LPS stimulation. (**A**) Synaptic development in xMG-transplanted retinal explants was analyzed by immunostaining with synaptic antibodies, anti-SV2 or -PSD95 (light blue). Scale bars, 20 µm. (**B**, **C**) Representative images illustrating engrafted synapse-specific proteins labeled by anti-SV2 or -PSD95 (light blue) in EGFP (green)-labeled xMG with anti-Iba1 (purple) outlining cell morphology at 7 days post-transplantation. Left panels show fluorescent images, while right panels depict orthogonal projection and 3D-surface images derived from the raw images. Rectangles highlight SV2 or PSD95 (light blue) engulfed within microglia (purple), respectively. Scale bars, 20 µm. (**D**) Immuno-Electron Microscopy images showing endogenous mouse microglia (mMG) and xeno-transplanted human microglia (xMG) (N, nucleus). The star indicates mitochondrial and the arrow indicates Golgi. Scale bars, 0.5–1 µm for low magnification, and 0.2 µm for high magnification. (**E**-**H**) Xeno-transplanted retinal explants were treated with 100 µg/ml LPS for 2 h. (**E**, **F**) Quantitative PCR was employed to analyze the relative expression of inflammatory-related genes using primers specific to mouse (m) and human (h). Data represent the mean value ± SEM. $n = 3$ independent biological repeats. (**G**) Representative images of EGFP (green)-labeled xMG with anti-Iba1 (purple) outlining cell morphology. Scale bars, 10 µm. (**H**) Statistical analysis of endpoint number in each xMG. Data represent the mean value ± SD. $n = 3$ retinas

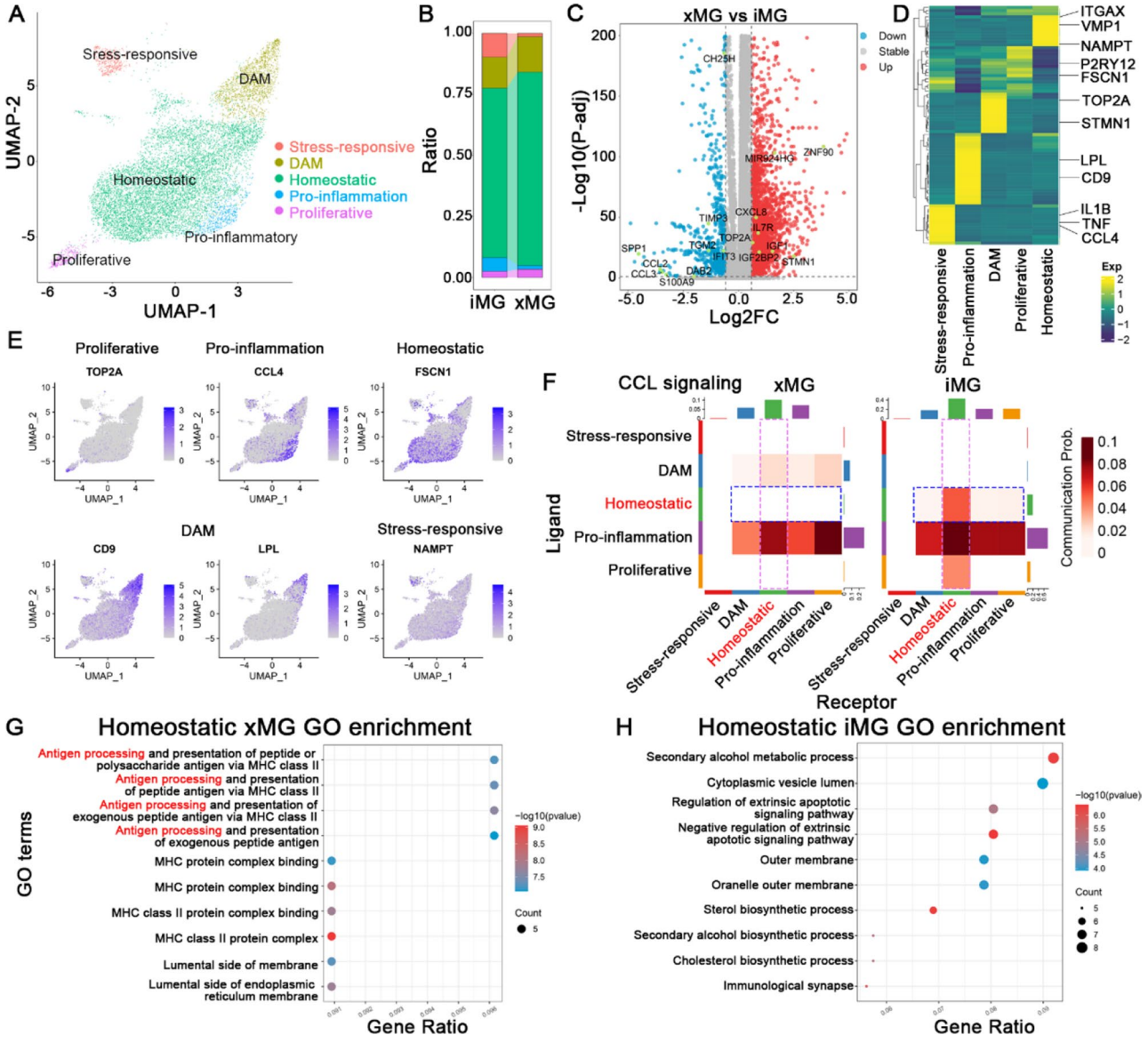

Fig. 3 Transcriptional changes after transplantation in retinal microenvironment. (**A**) Uniform Manifold Approximation and Projection (UMAP) plot showing the main cell types from xMG and iMG. Five types are colored and annotated based on feature gene expression. (**B**) Bar plot of the proportion of cells in each sample for each cell type identified. (**C**) Volcano plots showing differentially expressed genes (DEGs) between xMG and iMG. (**D**) Heatmap of differentially expressed marker genes for each cell type. (**E**) UMAP shows the expression of marker genes across the five cell types. (**F**) Heatmap of cell communication through the CCL signaling pathway between cell types in both xMG and iMG, analyzed using CellChat. (**G**, **H**) Top 10 Gene Oncology terms of homeostatic cells with upregulated genes in xMG and iMG

(Fig. 7A-C). xMG in the RGCL/IPL regions showed similar morphology in both Pde6b$^{-/-}$ and WT retinas (Fig. 7C). Additionally, activated xMG in the Pde6b$^{-/-}$ retina colocalized with RHO-positive signals, suggesting migration to lesioned photoreceptor cells (Fig. 7D, E). These findings demonstrate that xMG can be effectively applied to retinal degenerative models, offering a valuable approach for developing potential therapeutics.

Discussion

In this study, we introduced a novel approach to create a human microglia-mouse retina chimeric model through ex vivo co-culturing. We successfully transplanted and integrated iMG into mouse retinal explants, achieving over 86% replacement and maintaining the culture for up to 14 days. The resulting xMG exhibited typical microglial localization and retained essential functions such as proliferation, immune responsiveness, and synaptic pruning. This development is particularly significant because mouse microglia do not fully replicate the

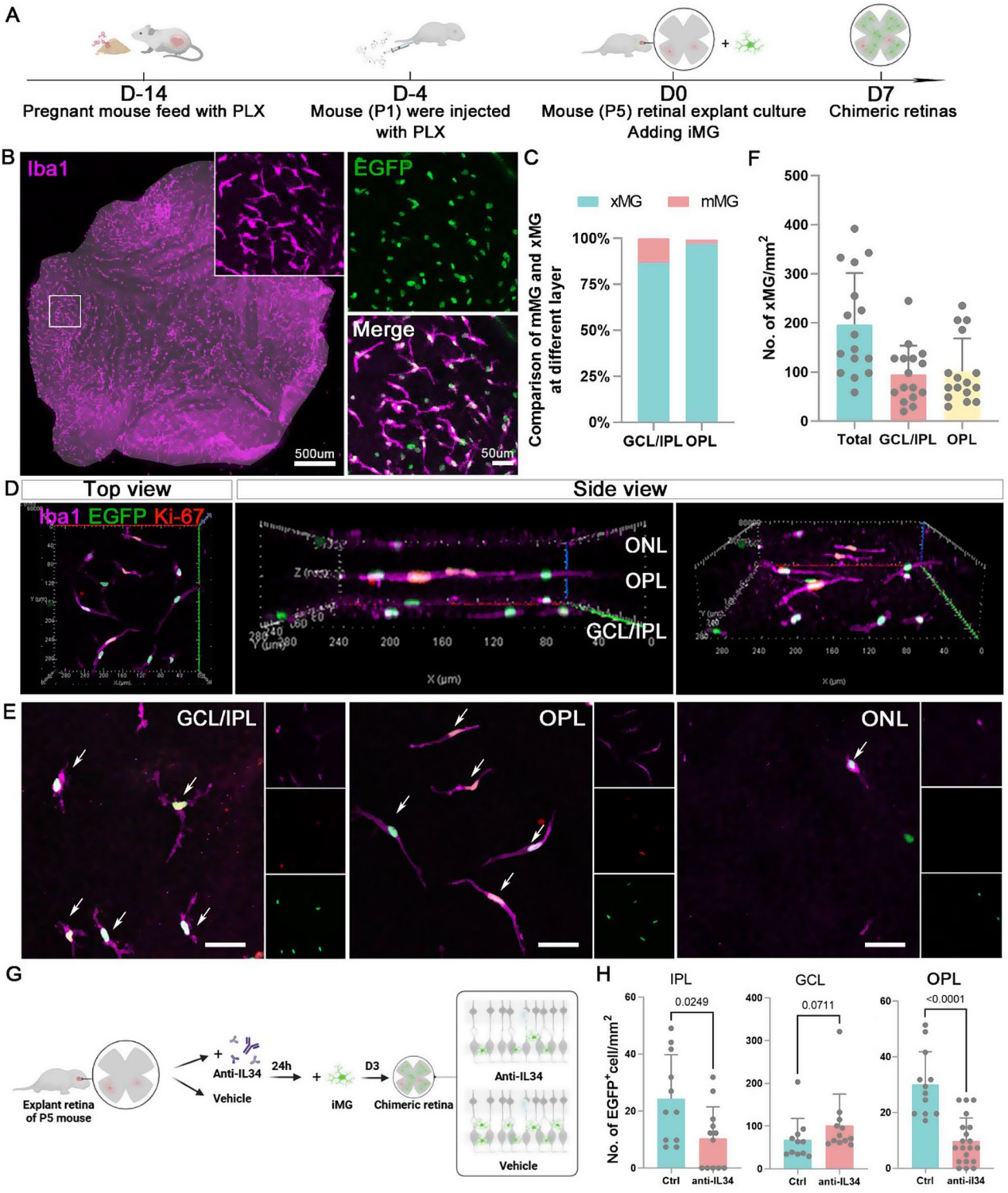

Fig. 4 (See legend on next page.)

(See figure on previous page.)

Fig. 4 xMG resemble their localization in the chimeric mouse retinal explants. (**A**) Schematic of the experimental design and procedures. Pregnant mice were fed PLX5622, and the neonatal mice were further injected with PLX5622 for 4 days. Explants transplanted with human iPSC-derived microglia (iMG) were cultured for 7 days. (**B**) Representative images of retinal whole mounts with anti-Iba1 immunostaining. Enlarged images show the co-labeling of EGFP (green) and Iba1 (purple). Scale bars, 500 μm and 50 μm in the original or enlarged images, respectively. (**C**) Quantitative analysis of replacement efficacy. Ratio of xeno-transplanted human microglia (xMG) to mouse endogenous microglia (mMG) in mouse retina explants. $n = 4$ retinas. (**D**) Representative 3D images (top view and side view) of image stacks showing xMG distribution at different layers in mouse retinal explants at 7 days post-transplantation. ONL: outer nuclear layer; OPL: outer plexiform layer; GCL/IPL: ganglion cell layer/inner plexiform layer. (**E**) Representative images from GCL/IPL, OPL, and ONL showing xMG (arrows indicated) morphology in mouse retinal explants. Scale bars, 50 μm. (**F**) Quantifications of xMG cell density in mouse retina explants. $n = 4$ retinas. (**G**) Schematic of the antibody (anti-IL34) blocking experiment procedures. (**H**) Quantification of xMG cell density in IPL, GCL, and OPL of mouse retinas in control and anti-IL34 treated groups. $n = 3$ retinas

characteristics of human microglia. Establishing such chimeric models greatly enhances our ability to study human microglia, providing a straightforward and accessible method that most laboratories can implement. Our model is poised to advance research into retinal microglia significantly.

While much of the existing research has focused on chimeric models of human microglia within the mouse brain, less attention has been given to the mouse retina. Recently, groundbreaking work demonstrated the successful integration of human iPSC-derived microglia into the adult mouse retina in vivo [22]. However, endogenous murine microglia can repopulate within 24 h after depletion, leaving a very narrow time window for the residency of transplanted microglia [47]. Moreover, subretinal transplantation in the adult retina requires the transplanted cells to pass through the outer nuclear layer (ONL) to reach the outer plexiform layer (OPL), which may damage the fragile photoreceptor cells [22]. Building on this foundation, we established a retinal chimeric model by co-culturing human iMG with mouse retinal explants by adding iMG to the ganglion cell layer (GCL) side, which mimics the microglial colonization during development [48, 49]. This approach provides a stable, simplified, and easy-to-handle method for establishing a human microglia-mouse retina chimeric model. However, ex vivo cultured retinal chimeric models face limitations, such as their inability to survive for several months, unlike in vivo conditions.

In vivo models enable xMG to survive for extended periods and reach higher levels of maturity, making them particularly suitable for studying chronic disease cycles and long-term cellular dynamics. However, these models typically require immunodeficient animals and involve complex transplantation surgeries, limiting their accessibility and scalability. Additionally, endogenous microglia repopulation within 24 h poses a challenge to maintaining transplanted xMG populations. Ex vivo models, on the other hand, avoid the need for immunodeficient animals and can be readily applied to established disease models, including human retinal organotypic cultures. They provide a simplified and highly controlled experimental environment, which is advantageous for short-term studies, such as drug screening, preclinical testing, and mechanistic analyses. However, the limited culture duration (up to 14 days) restricts their utility for investigating long-term disease processes or chronic conditions.

The success of our model depended on creating microglia-free niches, consistent with findings from previous studies [50, 51]. For microglial depletion in neonatal mice, we observed that microglial clearance through feeding pregnant female mice was more effective than intraperitoneal injection [52], leading to a higher survival rate of xMG. A previous study used 30 μM PLX3397 in the medium to deplete microglia in cultured mouse brain slices [25]. In our experiments, adding PLX5622 (3 μM) to the medium depleted endogenous microglia with regional variability, and increasing the concentration to 30 μM proved cytotoxic to the retina (data not shown). This could be due to the retina's increased sensitivity to small molecules or differences in the CSF inhibitors used [53, 54]. Further research is needed to clarify these findings.

Efficient depletion of endogenous microglia is critical for optimizing xMG transplantation and replacement efficiency. Consistent with prior studies, oral administration offers a safer and more scalable approach for long-term depletion protocols [47, 55, 56]. In contrast, intraperitoneal injections remain useful for short-term depletion but carry risks of toxicity and mortality in neonatal animals. Higher microglia depletion efficiency correlated with improved xMG migration and distribution in retinal explants. However, regions with incomplete microglia depletion exhibited limited xMG replacement, highlighting the importance of optimizing depletion protocols for robust transplantation outcomes. While oral PLX administration is preferable for studies requiring higher clearance efficiency and low mortality, intraperitoneal PLX injection may be used in short-term studies where partial depletion is sufficient. Future studies may explore combinatory approaches or alternative depletion strategies to further enhance efficiency and reproducibility.

Chemokine signaling plays a crucial role in regulating the chemotaxis of migrating microglia and is pivotal in neuroinflammation associated with neuronal disorders [57, 58]. Chemokine ligands and their corresponding receptors, such as CCR1, are key mediators in this

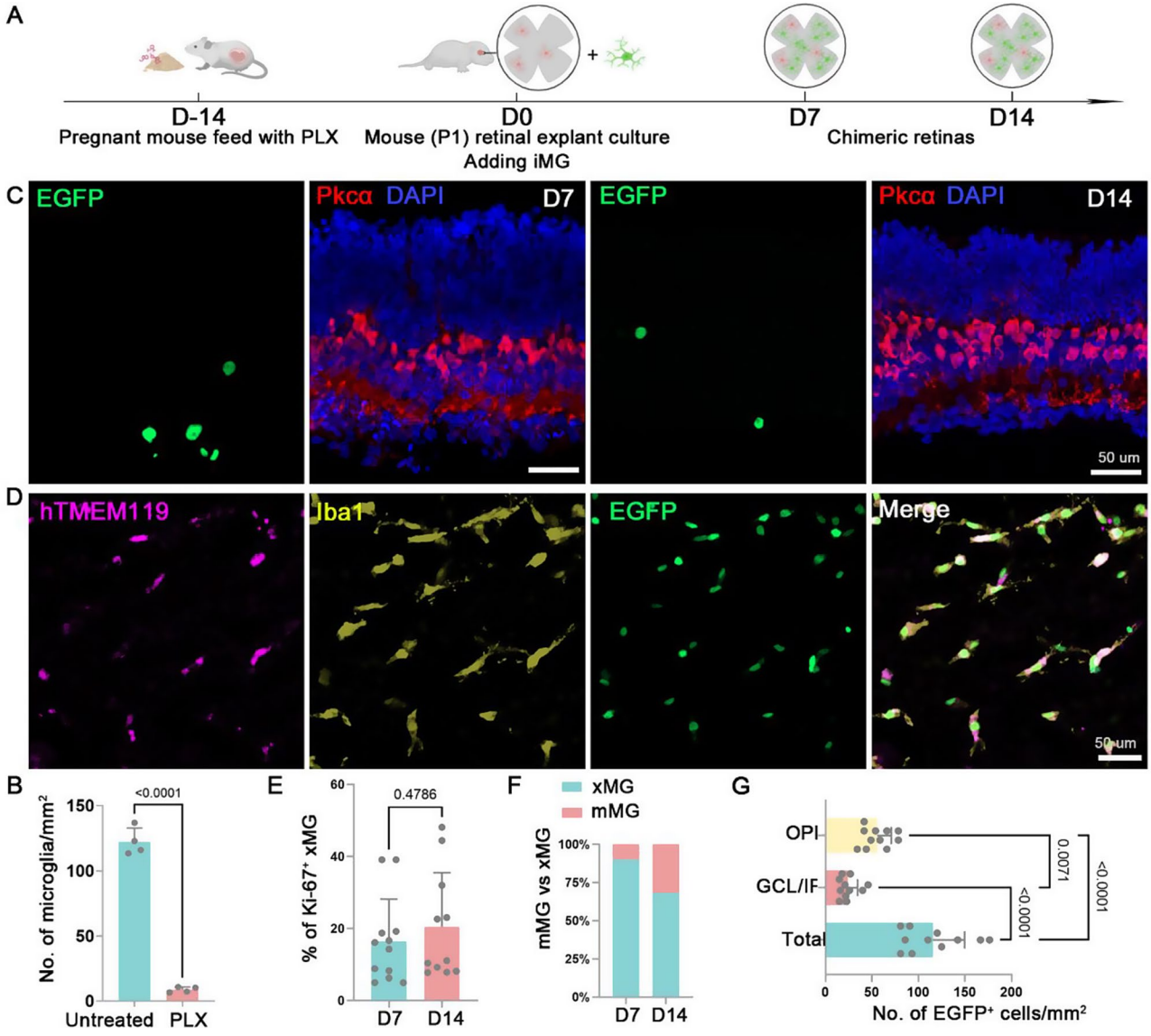

Fig. 5 Long-term culture of integrated xMG in chimeric mouse retinal explants. (**A**) Schematic of the experimental design and procedures. Pregnant mice were fed PLX5622, and the neonatal mice were subjected to retinal explant culture. Explants transplanted with human iPSC-derived microglia (iMG) were cultured for 7 or 14 days. (**B**) Quantitative analysis of microglia depletion in neonatal mice. (**C**) Immunofluorescent images depicting anti-PKCα (red) staining in retinal explant sections. 7 and 14 days after transplantation. Scale bars, 50 μm. (**D**) Representative images showing xMG in mouse retina explants expressing Iba1 and hTMEM119, a mature microglial marker. (**E**) Quantifications of Ki-67^{+} xMG percentage in total xMG of mouse retinal explants at 7 or 14 days post-transplantation. $n = 3$ retinas. (**F**) Quantitative analysis of replacement efficacy. The ratio of xMG to mouse endogenous microglia (mMG) in mouse retina explants at 7 days or 14 days post-transplantation. $n = 3$ retinas. (**G**) Quantifications of EGFP + cell density in different layers of mouse retinal explants at 14 days post-transplantation. $n = 3$ retinas

process and are essential for inflammatory responses [59]. When comparing homeostatic xMG and iMG, we found that the communication probability of CCL signaling (CCL8/CCL3/CCL13-CCR1) is higher in homeostatic iMG than that in xMG (Fig. 3F and S4A, B). Notably, the CCL8/CCL3/CCL13-CCR1 axis has been reported to be upregulated in several disease models, including multiple sclerosis [60], retinal degeneration [61], LPS-induced brain injury [62], and spinal cord injury [63]. Based on these findings, homeostatic iMG appear to adopt a more inflammatory profile, whereas xMG may more closely resemble homeostatic microglia.

Microglia are known to self-renew through proliferation under both physiological and pathological conditions [64–66]. Our findings showed that xMG maintained their proliferative activity within the mouse retina explants, ensuring the stability and sustainability of microglial populations over time. During extended culture periods, these xMG gradually matured and adopted a homeostatic morphology. Inflammatory responses in the CNS can

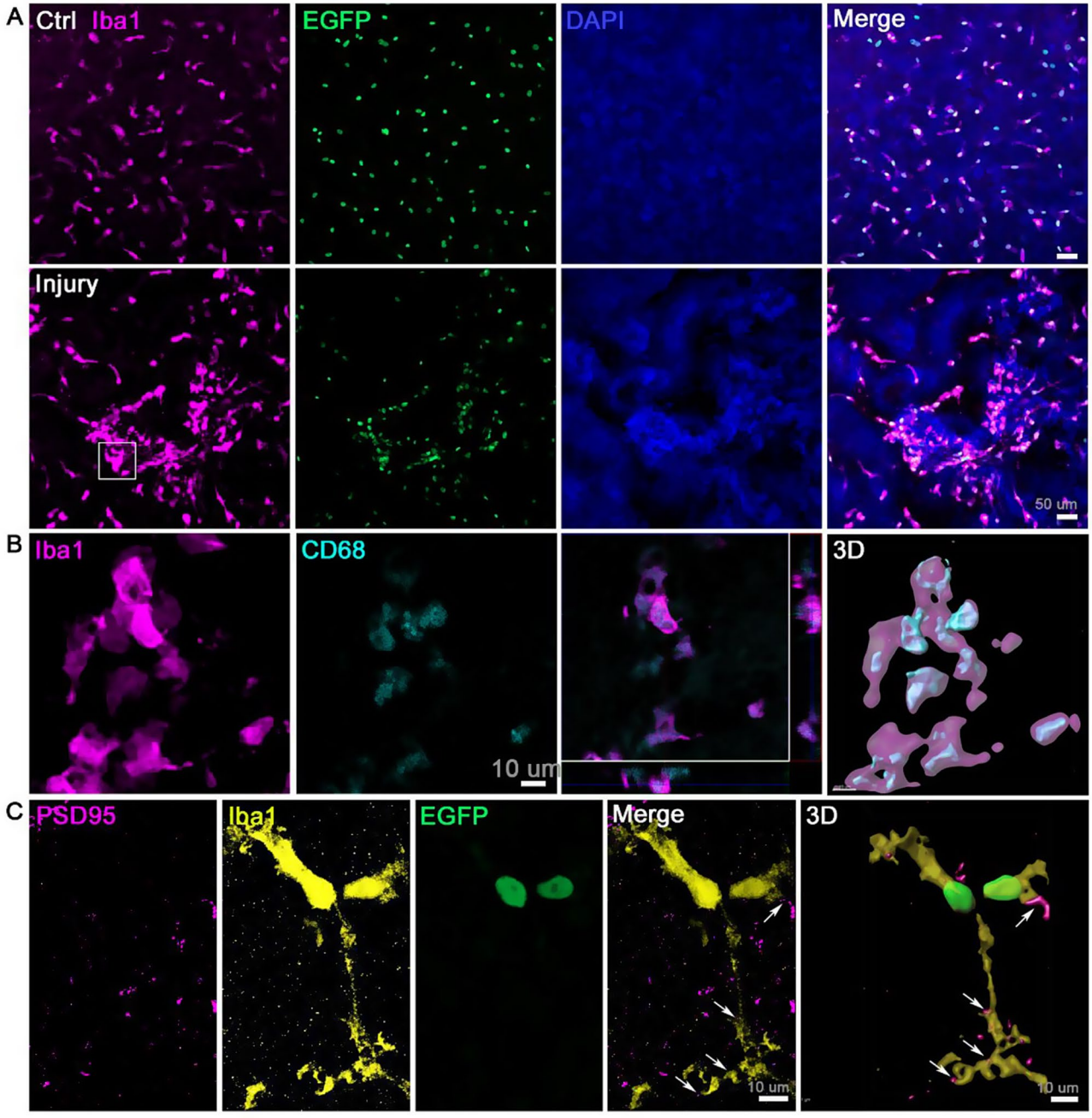

Fig. 6 Function of long-lived xMG in chimeric mouse retinal explants. (**A**) Representative images showing xMG distribution in mouse retina explants at non-injury and the injury site. xMG aggregate around the injury site. Scale bars, 50 μm. (**B**) Representative images showing phagosome labeled by anti-CD68 (light blue) in xMG with anti-Iba1 (purple) outlining cell morphology at 14 days post-transplantation. Left panels display fluorescent images, while the right panels depict 3D-surface images derived from the raw images. (**C**) Representative images showing PSD95-positive puncta engrafted in $EGFP^+$ xMG with anti-Iba1 (yellow) outlining cell morphology in a mouse retinal explant at 14 days post-transplantation. The left panels show fluorescent images (arrows indicated engrafted puncta), while the right panels depict 3D-surface images derived from the raw images. Scale bars, 10 μm

significantly enhance microglial proliferation [67, 68]. In our ex vivo retinal chimeric model, exogenous microglia retained proliferative ability after transplantation. Further research is required to identify additional factors that may regulate xMG proliferation.

Conclusion

Overall, our chimeric model provides a valuable platform for studying human microglia in a retinal context and offers potential insights for developing therapies for retinal degenerative diseases. In future research, we can utilize iPSCs from patients with retina-related diseases

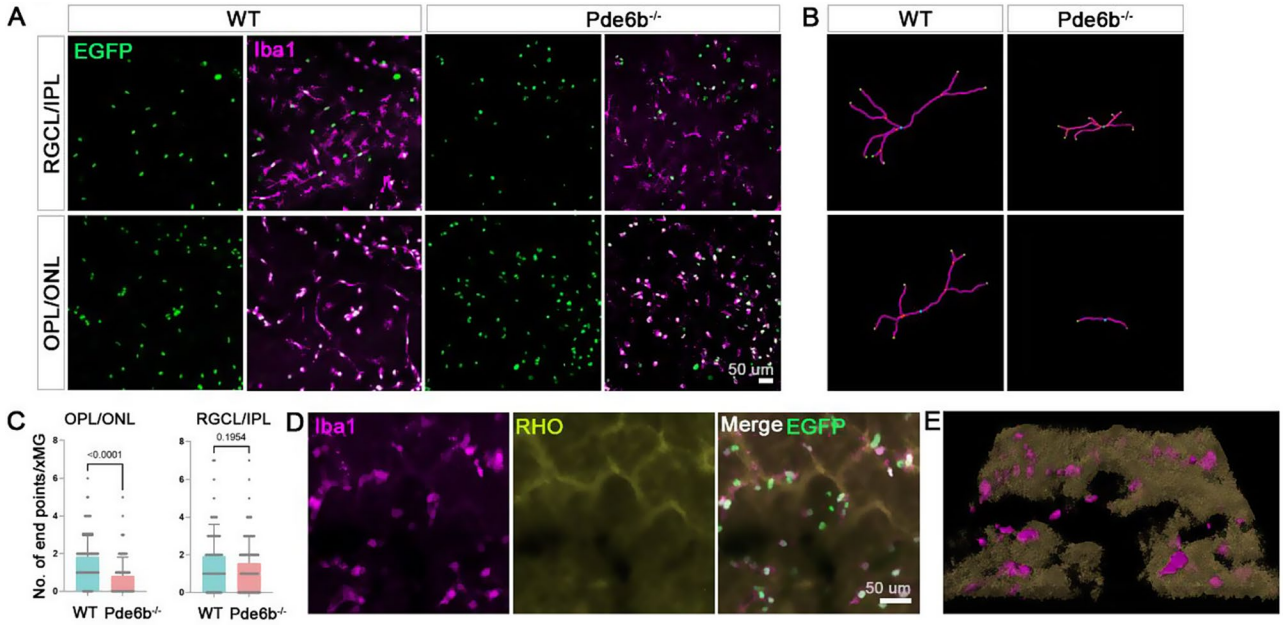

Fig. 7 Activation of xMG in the ONL of Pde6b$^{-/-}$ retina explants. (**A**) Representative images showing the distribution of xMG in mouse retinal explants at both non-injury and injury sites, with xMG aggregating around the injury site. Scale bars, 50 μm. (**B**) Comparison of microglial morphology in wild-type (WT) and Pde6b$^{-/-}$ retinas, including 3D reconstructions of single xMG in the RGCL/IPL and OPL/ONL regions. (**C**) Statistical analysis of the number of endpoints in each microglia. (**D**) Iba1^{+} and EGFP^{+} xMG are present in the RHO^{+} photoreceptor cell layer. Scale bar, 50 μm. (**E**) 3D reconstruction of the image in (**D**)

to investigate whether their disease-specific microglia can induce microglia-related conditions in a healthy isolated retina. This approach will help elucidate the specific pathogenesis of microglia-related diseases. In conclusion, the successful establishment of the exogenous microglial retinal chimerism model provides substantial support for future in vitro studies of microglia in the retina, advancing our understanding and potential treatment of retinal diseases.

Supplementary Information

The online version contains supplementary material available at https://doi.org/10.1186/s12974-025-03393-8.

Supplementary Material 1

Acknowledgements
We are grateful to the Scientific Research Center of Wenzhou Medical University for instruments supporting this work. We thank Miss Yizhen Zhang for her significant comments and helpful discussion. This work was supported in part by grants from Natural Science Foundation of China (82070981), State Key Laboratory of Neuroscience (SKLN-202103), National Key Research and Development Program of China (2022YFA1105503), Zhejiang Natural Science Foundation of China (LY22H120008), Wenzhou Association for Science and Technology (kjfw27), Scientific Research Program of Wenzhou (Y2023172, Y20240060), Start-up Foundation of Wenzhou Medical University (89219003).

Author contributions
MLG, JZ, and JQ designed and supervised the experiments. CT performed stem cell differentiation. CT, QYL, and QQZ performed explant culture, part immunofluorescence, and qPCR. BLR and YYJ provided animals and performed dissection. JZ and CT completed electron microscopy. MLG conducted data and image analysis. ZCL, LL and YAJ performed part immunofluorescence and quantification. XFH and BZP performed single-cell sorting and scRNA-seq data analysis. TC wrote the draft of the manuscript. MLG and JZ wrote the final manuscript. All authors approved the final manuscript.

Data availability
Availability of data and materialsThe single-cell RNA sequencing datasets generated in this study has been uploaded in the Genome Sequence Archive for human (https://ngdc.cncb.ac.cn/gsa-human/) and the accession number is HRA008598.

Declarations

Ethical approval
The human iPSC cell lines used in this study were purchased from Nuwacell® (RC01010, RC01001-A, Hefei, China). Neither human ethical issues were involved. The animal experiment procedures were conducted in accordance with the guidelines approved by the Animal Ethics Committee of Wenzhou Medical University (approval number wydw2023-0321).

Competing interests
The authors declare no competing interests.

Author details
[1]The State Key Laboratory of Ophthalmology, Optometry and Visual Science, Wenzhou Medical University, Wenzhou 325027, China
[2]Laboratory of Retinal Physiology and Disease, Eye Hospital and School of Ophthalmology and Optometry, Wenzhou Medical University, Wenzhou 325027, China
[3]Zhejiang Provincial Clinical Research Center for Pediatric Disease, The Second Affiliated Hospital and Yuying Children's Hospital of Wenzhou Medical University, Wenzhou 325027, China
[4]The State Key Laboratory of Ophthalmology, Optometry and Vision Science, Wenzhou Medical University, Wenzhou 325027, China
[5]Lead Contact, Laboratory of Retinal Physiology and Disease, Eye Hospital and School of Ophthalmology and Optometry, Wenzhou Medical University, Wenzhou, Zhejiang 325027, China

[6]Laboratory of Retinal Physiology and Disease, Eye Hospital and School of Ophthalmology and Optometry, Wenzhou Medical University, Wenzhou, Zhejiang 325027, China

Received: 22 November 2024 / Accepted: 20 February 2025
Published online: 27 February 2025

References

1. Colonna M. Butovsky. Microglia function in the central nervous system during health and neurodegeneration. Annu Rev Immunol. 2017;35:441–68. https://doi.org/10.1146/annurev-immunol-051116-052358.
2. McQuade A, Kang YJ, Hasselmann J, Jairaman A, Sotelo A, Coburn M, et al. Gene expression and functional deficits underlie TREM2-knockout microglia responses in human models of Alzheimer's disease. Nat Commun. 2020;11:5370. https://doi.org/10.1038/s41467-020-19227-5.
3. Saijo K, Glass CK. Microglial cell origin and phenotypes in health and disease. Nat Rev Immunol. 2011;11:775–87. https://doi.org/10.1038/nri3086.
4. Rathnasamy G, Foulds WS, Ling EA. Kaur. Retinal microglia - A key player in healthy and diseased retina. Prog Neurobiol. 2019;173:18–40. https://doi.org/10.1016/j.pneurobio.2018.05.006.
5. Karlstetter M, Scholz R, Rutar M, Wong WT, Provis JM, Langmann T. Retinal microglia: just bystander or target for therapy? Prog Retin Eye Res. 2015;45:30–57. https://doi.org/10.1016/j.preteyeres.2014.11.004.
6. Fritsche LG, Igl W, Bailey JNC, Grassmann F, Sengupta S, Bragg-Gresham JL, et al. A large genome-wide association study of age-related macular degeneration highlights contributions of rare and common variants. Nat Genet. 2016;48:134–43. https://doi.org/10.1038/ng.3448.
7. Fritsche LG, Fariss RN, Stambolian D, Abecasis GR, Curcio CA, Swaroop A. Age-related macular degeneration: genetics and biology coming together. Annu Rev Genomics Hum Genet. 2014;15:151–71. https://doi.org/10.1146/annurev-genom-090413-025610.
8. Gold B, Merriam JE, Zernant J, Hancox LS, Taiber AJ, Gehrs K, et al. Variation in factor B (BF) and complement component 2 (C2) genes is associated with age-related macular degeneration. Nat Genet. 2006;38:458–62.
9. Pauly D, Agarwal D, Dana N, Schäfer N, Biber J, Wunderlich KA, et al. Cell-Type-Specific complement expression in the healthy and diseased retina. Cell Rep. 2019;29. https://doi.org/10.1016/j.celrep.2019.10.084.
10. Hasselmann J, Blurton-Jones M. Human iPSC-derived microglia: A growing toolset to study the brain's innate immune cells. Glia. 2020;68:721–39. https://doi.org/10.1002/glia.23781.
11. Masuda T, Sankowski R, Staszewski O, Böttcher C, Amann L, Sagar, et al. Spatial and Temporal heterogeneity of mouse and human microglia at single-cell resolution. Nature. 2019;566:388–92. https://doi.org/10.1038/s41586-019-0924-x.
12. Gosselin D, Skola D, Coufal NG, Holtman IR, Schlachetzki JCM, Sajti E, et al. An environment-dependent transcriptional network specifies human microglia identity. Science. 2017;356. https://doi.org/10.1126/science.aal3222.
13. Abud EM, Ramirez RN, Martinez ES, Healy LM, Nguyen CHH, Newman SA, et al. iPSC-Derived human Microglia-like cells to study neurological diseases. Neuron. 2017;94. https://doi.org/10.1016/j.neuron.2017.03.042.
14. Popova G, Soliman SS, Kim CN, Keefe MG, Hennick KM, Jain S, et al. Human microglia States are conserved across experimental models and regulate neural stem cell responses in chimeric organoids. Cell Stem Cell. 2021;28. https://doi.org/10.1016/j.stem.2021.08.015.
15. Speicher AM, Wiendl H, Meuth SG. Pawlowski. Generating microglia from human pluripotent stem cells: novel in vitro models for the study of neurodegeneration. Mol Neurodegener. 2019;14:46. https://doi.org/10.1186/s13024-019-0347-z.
16. Pandya H, Shen MJ, Ichikawa DM, Sedlock AB, Choi Y, Johnson KR, et al. Differentiation of human and murine induced pluripotent stem cells to microglia-like cells. Nat Neurosci. 2017;20:753–9. https://doi.org/10.1038/nn.4534.
17. Muffat J, Li Y, Yuan B, Mitalipova M, Omer A, Corcoran S, et al. Efficient derivation of microglia-like cells from human pluripotent stem cells. Nat Med. 2016;22:1358–67. https://doi.org/10.1038/nm.4189.
18. Takata K, Kozaki T, Lee CZW, Thion MS, Otsuka M, Lim S, et al. Induced-Pluripotent-Stem-Cell-Derived primitive macrophages provide a platform for modeling Tissue-Resident macrophage differentiation and function. Immunity. 2017;47:183–e198186. https://doi.org/10.1016/j.immuni.2017.06.017.
19. Mancuso R, Van Den Daele J, Fattorelli N, Wolfs L, Balusu S, Burton O, et al. Stem-cell-derived human microglia transplanted in mouse brain to study human disease. Nat Neurosci. 2019;22:2111–6. https://doi.org/10.1038/s41593-019-0525-x.
20. Hasselmann J, Coburn MA, England W, Figueroa Velez DX, Kiani Shabestari S, Tu CH, et al. Development of a chimeric model to study and manipulate human microglia in vivo. Neuron. 2019;103:1016–e10331010. https://doi.org/10.1016/j.neuron.2019.07.002.
21. Xu R, Li X, Boreland AJ, Posyton A, Kwan K, Hart RP, et al. Human iPSC-derived mature microglia retain their identity and functionally integrate in the chimeric mouse brain. Nat Commun. 2020;11:1577. https://doi.org/10.1038/s41467-020-15411-9.
22. Ma W, Zhao L, Xu B, Fariss RN, Redmond TM, Zou J et al. Human iPSC-derived microglial cells integrated into mouse retina and recapitulated features of endogenous microglia. Elife. 2024;12:RP90695. https://doi.org/10.7554/eLife.90695
23. Svoboda DS, Barrasa MI, Shu J, Rietjens R, Zhang S, Mitalipova M, et al. Human iPSC-derived microglia assume a primary microglia-like state after transplantation into the neonatal mouse brain. Proc Natl Acad Sci U S A. 2019;116:25293–303. https://doi.org/10.1073/pnas.1913541116.
24. Dionisio-Santos DA, Olschowka JA. O'Banion. Exploiting microglial and peripheral immune cell crosstalk to treat Alzheimer's disease. J Neuroinflammation. 2019;16:74. https://doi.org/10.1186/s12974-019-1453-0.
25. Ogaki A, Ikegaya Y. Koyama. Replacement of mouse microglia with human induced pluripotent stem cell (hiPSC)-Derived microglia in mouse organotypic slice cultures. Front Cell Neurosci. 2022;16:918442. https://doi.org/10.3389/fncel.2022.918442.
26. Schnichels S, Schultheiss M, Klemm P, Blak M, Herrmann T, Melchinger M, et al. Cyclosporine A protects retinal explants against hypoxia. Int J Mol Sci. 2021;22. https://doi.org/10.3390/ijms221910196.
27. Hurst J, Mueller-Buehl AM, Hofmann L, Kuehn S, Herms F, Schnichels S, et al. iNOS-inhibitor driven neuroprotection in a Porcine retina organ culture model. J Cell Mol Med. 2020;24:4312–23. https://doi.org/10.1111/jcmm.15091.
28. Gao M-L, Zhang X, Han F, Xu J, Yu S-J, Jin K, et al. Functional microglia derived from human pluripotent stem cells empower retinal organ. Sci China Life Sci. 2022;65:1057–71. https://doi.org/10.1007/s11427-021-2086-0.
29. Gao ML, Wang TY, Lin X, Tang C, Li M, Bai ZP, et al. Retinal organoid microenvironment enhanced bioactivities of Microglia-Like cells derived from HiPSCs. Invest Ophthalmol Vis Sci. 2024;65:19. https://doi.org/10.1167/iovs.65.12.19.
30. Liu X, Rao B, Lin Q, Gao M. Zhang. Preparing retinal organoid samples for transmission Electron microscopy. J Vis Exp. 2024. https://doi.org/10.3791/66590.
31. Erblich B, Zhu L, Etgen AM, Dobrenis K, Pollard JW. Absence of colony stimulation factor-1 receptor results in loss of microglia, disrupted brain development and olfactory deficits. PLoS ONE. 2011;6:e26317. https://doi.org/10.1371/journal.pone.0026317.
32. Rathinam C, Poueymirou WT, Rojas J, Murphy AJ, Valenzuela DM, Yancopoulos GD, et al. Efficient differentiation and function of human macrophages in humanized CSF-1 mice. Blood. 2011;118:3119–28. https://doi.org/10.1182/blood-2010-12-326926.
33. Schafer DP, Lehrman EK, Kautzman AG, Koyama R, Mardinly AR, Yamasaki R, et al. Microglia sculpt postnatal neural circuits in an activity and complement-dependent manner. Neuron. 2012;74:691–705. https://doi.org/10.1016/j.neuron.2012.03.026.
34. Rich KA, Zhan Y, Blanks JC. Migration and synaptogenesis of cone photoreceptors in the developing mouse retina. J Comp Neurol. 1997;388:47–63.
35. Van Der Voorn P, Tekstra J, Beelen RHJ, Tensen CP, Van Der Valk P. De Groot. Expression of MCP-1 by reactive astrocytes in demyelinating multiple sclerosis lesions. Am J Pathol. 1999;154:45–51. https://doi.org/10.1016/s0002-9440(10)65249-2.
36. Zhou ZH, Han Y, Wei T, Aras S, Chaturvedi P, Tyler S, et al. Regulation of monocyte chemoattractant protein (MCP)-1 transcription by interferon-gamma (IFN-gamma) in human Astrocytoma cells: postinduction refractory state of the gene, governed by its upstream elements. FASEB J. 2001;15:383–92.
37. Fain JN, Madan AK. Regulation of monocyte chemoattractant protein 1 (MCP-1) release by explants of human visceral adipose tissue. Int J Obes. 2005;29:1299–307. https://doi.org/10.1038/sj.ijo.0803032.
38. Marsh SE, Walker AJ, Kamath T, Dissing-Olesen L, Hammond TR, de Soysa TY, et al. Dissection of artifactual and confounding glial signatures by single-cell sequencing of mouse and human brain. Nat Neurosci. 2022;25:306–16. https://doi.org/10.1038/s41593-022-01022-8.

39. Benhar I, Ding J, Yan W, Whitney IE, Jacobi A, Sud M, et al. Temporal single-cell atlas of non-neuronal retinal cells reveals dynamic, coordinated multicellular responses to central nervous system injury. Nat Immunol. 2023;24:700–13. https://doi.org/10.1038/s41590-023-01437-w.
40. Umpierre AD, Wu LJ. How microglia sense and regulate neuronal activity. Glia. 2021;69:1637–53. https://doi.org/10.1002/glia.23961.
41. Hammond B.P., Manek R, Kerr BJ, Macauley MS, Plemel JR. Regulation of microglia population dynamics throughout development, health, and disease. Glia. 2021;69:2771–97. https://doi.org/10.1002/glia.24047.
42. O'Koren EG, Yu C, Klingeborn M, Wong AYW, Prigge CL, Mathew R, et al. Microglial function is distinct in different anatomical locations during retinal homeostasis and degeneration. Immunity. 2019;50. https://doi.org/10.1016/j.immuni.2019.02.007.
43. Müller B, Wagner F, Lorenz B, Stieger K. Organotypic cultures of adult mouse retina: morphologic changes and gene expression. Investig Ophthalmol Vis Sci. 2017;58:1930–40. https://doi.org/10.1167/iovs.16-20718.
44. Schnichels S, Paquet-Durand F, Loscher M, Tsai T, Hurst J, Joachim SC, et al. Retina in a dish: cell cultures, retinal explants and animal models for common diseases of the retina. Prog Retin Eye Res. 2021;81:100880. https://doi.org/10.1016/j.preteyeres.2020.100880.
45. Bennett ML, Bennett FC, Liddelow SA, Ajami B, Zamanian JL, Fernhoff NB, et al. New tools for studying microglia in the mouse and human CNS. Proc Natl Acad Sci USA. 2016;113:E1738–46. https://doi.org/10.1073/pnas.1525528113.
46. White DT, Sengupta S, Saxena MT, Xu Q, Hanes J, Ding D, et al. Immunomodulation-accelerated neuronal regeneration following selective rod photoreceptor cell ablation in the zebrafish retina. Proc Natl Acad Sci U S A. 2017;114. https://doi.org/10.1073/pnas.1617721114.
47. Huang Y, Xu Z, Xiong S, Sun F, Qin G, Hu G, et al. Repopulated microglia are solely derived from the proliferation of residual microglia after acute depletion. Nat Neurosci. 2018;21:530–40. https://doi.org/10.1038/s41593-018-0090-8.
48. Diaz-Araya CM, Provis JM, Penfold PL, Billson FA. Development of microglial topography in human retina. J Comp Neurol. 1995;363:53–68. https://doi.org/10.1002/cne.903630106.
49. Silverman SM, Wong WT. Microglia in the retina: roles in development, maturity, and disease. Annu Rev Vis Sci. 2018;4:45–77. https://doi.org/10.1146/annurev-vision-091517-034425.
50. Xu Z, Rao Y, Huang Y, Zhou T, Feng R, Xiong S, et al. Efficient strategies for microglia replacement in the central nervous system. Cell Rep. 2020;32:108041. https://doi.org/10.1016/j.celrep.2020.108041.
51. Rao Y, Peng B. Allogenic microglia replacement: A novel therapeutic strategy for neurological disorders. Fundam Res. 2024;4:237–45. https://doi.org/10.1016/j.fmre.2023.02.025.
52. Rosin JM, Vora SR, Kurrasch DM. Depletion of embryonic microglia using the CSF1R inhibitor PLX5622 has adverse sex-specific effects on mice, including accelerated weight gain, hyperactivity and anxiolytic-like behaviour. Brain Behav Immun. 2018;73:682–97. https://doi.org/10.1016/j.bbi.2018.07.023.
53. Liu Y, Given KS, Dickson EL, Owens GP, Macklin WB, Bennett JL. Concentration-dependent effects of CSF1R inhibitors on oligodendrocyte progenitor cells ex vivo and in vivo. Exp Neurol. 2019;318:32–41. https://doi.org/10.1016/j.expneurol.2019.04.011.
54. Okojie AK, Uweru JO, Coburn MA, Li S, Cao-Dao VD, Eyo UB. Distinguishing the effects of systemic CSF1R Inhibition by PLX3397 on microglia and peripheral immune cells. J Neuroinflammation. 2023;20:242. https://doi.org/10.1186/s12974-023-02924-5.
55. Spangenberg E, Severson PL, Hohsfield LA, Crapser J, Zhang J, Burton EA, et al. Sustained microglial depletion with CSF1R inhibitor impairs parenchymal plaque development in an Alzheimer's disease model. Nat Commun. 2019;10:3758. https://doi.org/10.1038/s41467-019-11674-z.
56. Wei M, Zhang G, Huang Z, Ding X, Sun Q, Zhang Y, et al. ATP-P2X(7)R-mediated microglia senescence aggravates retinal ganglion cell injury in chronic ocular hypertension. J Neuroinflammation. 2023;20:180. https://doi.org/10.1186/s12974-023-02855-1.
57. Thergarajan P, O'Brien TJ, Jones NC, Ali I. Ligand-receptor interactions: A key to Understanding microglia and astrocyte roles in epilepsy. Epilepsy Behavior: E&B. 2024;163:110219. https://doi.org/10.1016/j.yebeh.2024.110219.
58. Lau SF, Fu AKY, Ip NY. Receptor-ligand interaction controls microglial chemotaxis and amelioration of Alzheimer's disease pathology. J Neurochem. 2023;166:891–903. https://doi.org/10.1111/jnc.15933.
59. Tian Q, Yan Z, Guo Y, Chen Z, Li M. Inflammatory role of CCR1 in the central nervous system. Neuroimmunomodulation. 2024;31:173–82. https://doi.org/10.1159/000540460.
60. Banisor I, Leist TP, Kalman B. Involvement of beta-chemokines in the development of inflammatory demyelination. J Neuroinflammation. 2005;2:7. https://doi.org/10.1186/1742-2094-2-7.
61. Kohno H, Meada T, Perusek L, Pearlman E, Meada A.CCL3 production by microglial cells modulates disease severity in murine models of retinal degeneration. J Immunol. 2014;192(8):3816-27. https://doi.org/10.4049/jimmunol.1301738
62. Zhu X, Wei D, Chen O, Zhang Z, Xue J, Huang S, et al. Upregulation of CCL3/MIP-1alpha regulated by MAPKs and NF-kappaB mediates microglial inflammatory response in LPS-induced brain injury. Acta Neurobiol Exp. 2016;76:304–17. https://doi.org/10.21307/ane-2017-029.
63. Knerlich-Lukoschus F, von der Ropp-Brenner B, Lucius R, Mehdorn HM. Held-Feindt. Spatiotemporal CCR1, CCL3(MIP-1α), CXCR4, CXCL12(SDF-1α) expression patterns in a rat spinal cord injury model of posttraumatic neuropathic pain. J Neurosurg Spine. 2011;14:583–97. https://doi.org/10.3171/2010.12.Spine10480.
64. Ajami B, Bennett JL, Krieger C, Tetzlaff W, Rossi FM. Local self-renewal can sustain CNS microglia maintenance and function throughout adult life. Nat Neurosci. 2007;10:1538–43. https://doi.org/10.1038/nn2014.
65. Bruttger J, Karram K, Wortge S, Regen T, Marini F, Hoppmann N, et al. Genetic cell ablation reveals clusters of local Self-Renewing microglia in the mammalian central nervous system. Immunity. 2015;43:92–106. https://doi.org/10.1016/j.immuni.2015.06.012.
66. Jin N, Gao L, Fan X. Xu. Friend or foe?? Resident microglia vs bone Marrow-Derived microglia and their roles in the retinal degeneration. Mol Neurobiol. 2017;54:4094–112. https://doi.org/10.1007/s12035-016-9960-9.
67. Gomez-Nicola D, Fransen NL, Suzzi S, Perry VH. Regulation of microglial proliferation during chronic neurodegeneration. J Neurosci. 2013;33:2481–93. https://doi.org/10.1523/JNEUROSCI.4440-12.2013.
68. Kokkosis AG, Madeira MM, Hage Z, Valais K, Koliatsis D, Resutov E, et al. Chronic psychosocial stress triggers microglial-/macrophage-induced inflammatory responses leading to neuronal dysfunction and depressive-related behavior. Glia. 2024;72:111–32. https://doi.org/10.1002/glia.24464.

Publisher's note